



A complete analytical study on the dynamics of simple chaotic systems

G SIVAGANESH¹, A ARULGNANAM² * and A N SEETHALAKSHMI³

¹Department of Physics, Alagappa Chettiar Government College of Engineering and Technology, Karaikudi 630 004, India

²Department of Physics, St. John's College (affiliated to Manonmaniam Sundaranar University, Abishekapatti, Tirunelveli 627 012, India), Palayamkottai 627 002, India

³Department of Physics, The M.D.T. Hindu College (affiliated to Manonmaniam Sundaranar University, Abishekapatti, Tirunelveli 627 012, India), Tirunelveli 627 010, India

*Corresponding author. E-mail: gospelin@gmail.com

MS received 9 February 2018; revised 13 August 2018; accepted 20 August 2018;
published online 1 February 2019

Abstract. We report, in this paper, a complete analytical study on the bifurcations and chaotic phenomena observed in certain second-order, non-autonomous, dissipative chaotic systems. One-parameter bifurcation diagrams obtained from the analytical solutions revealing several chaotic phenomena such as antimonotonicity, period-doubling sequences and Feignbaum remerging have been presented. Further, the analytical solutions are used to obtain basins of attraction, phase portraits and Poincare maps for different chaotic systems. Experimentally observed chaotic attractors in some of the systems are presented to confirm the analytical results. The bifurcations and chaotic phenomena studied through explicit analytical solutions are reported in the literature for the first time.

Keywords. Chaos; antimonotonicity; piecewise linear.

PACS Nos 05.45.–a; 05.45.Ac

1. Introduction

Chaos in electronic circuits has been a topic of interest among researchers because of its application to secure communication [1–3]. After the observation of a chaotic attractor in an autonomous circuit system by Matsumoto [4], several electronic circuits with chaotic dynamics have been reported [5–10]. The implementation of the Chua's diode using Op-Amps [11] enabled researchers to identify different types of nonlinear elements [6,12]. Even though a large volume of research is done in chaos theory, only a few have reported analytical studies on chaos and its synchronisation. The analytical results thus obtained have been used to study chaos and synchronisation through phase portraits [6–8,13–20]. Being the prime validation for analysing the dynamics of chaotic systems, the explicit analytical solutions play an important role in the study of chaotic systems. However, a complete analytical study on the evolution and characterisation of chaos through bifurcation diagrams, basins of attraction and Poincare maps obtained from analytical solutions is rare in the

literature. Hence, an explicit analytical solution revealing the chaotic behaviours of dynamical systems seems to be much important and has to be focussed greatly for its extensive applications. Such a potential explicit analytical solution producing several chaotic behaviours and their characterisations is presented and discussed in this paper.

A complete analytical study on the chaotic dynamics of a class of second-order, non-autonomous systems with piecewise-linear nonlinear elements is presented in this paper. Nonlinear circuit elements with three segmented $V-I$ characteristics have been considered for the present study. The dynamics of these systems have been studied by presenting one-parameter bifurcation diagrams, phase portraits, basins of attraction, Poincare maps and power spectrum obtained from the analytical solutions. Further, some of the significant phenomena observed in these chaotic systems have been studied through analytical solutions. The coexistence of chaotic attractors arising from different basins of attractions is presented. The chaotic attractors produced by coupling the analytical solutions obtained in each of the

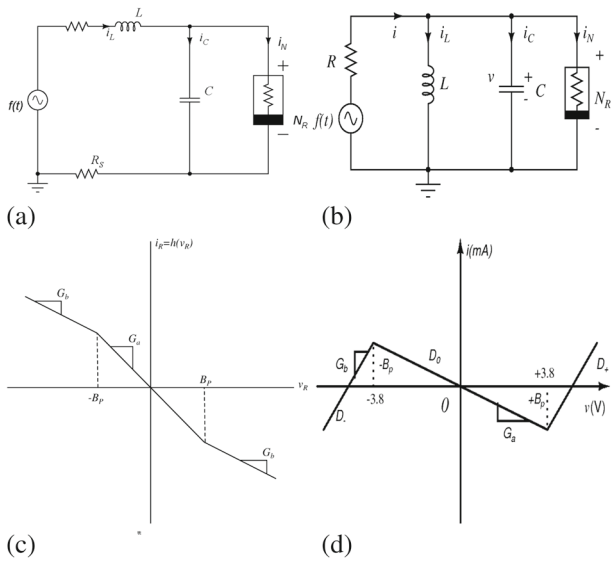


Figure 1. Schematic representation of the sinusoidally forced (a) series LCR circuit with a nonlinear element N_R connected parallel to the capacitor, (b) parallel LCR circuit with a nonlinear element N_R , (c) $V-I$ characteristics of the Chua's diode with three negative slope regions and (d) $V-I$ characteristics of the simplified nonlinear element with two positive outer slopes and one negative inner slope.

piecewise-linear regions are presented for each chaotic system.

For the present study, we consider two types of second-order chaotic circuit systems, each with two different nonlinear elements. Figures 1a and 1b show the schematic representation of the sinusoidally forced series and parallel LCR circuits with piecewise-linear elements N_R . The nonlinear element may be a Chua's diode [11] or a simplified nonlinear element [6]. The $V-I$ characteristics of the Chua's diode and the simplified nonlinear element are shown in figures 1c and 1d, respectively. The paper is divided into two sections. In §2, we present the generalised analytical solutions for series LCR circuit systems with piecewise-linear nonlinear elements and the analytical dynamics of two types of circuit systems. In §3, the generalised analytical solutions and analytical dynamics of the parallel LCR circuit systems are presented.

2. Analytical dynamics of the series LCR circuit systems

The circuit equations for a sinusoidally forced series LCR circuit with any three-segmented, piecewise-linear, voltage-controlled nonlinear element are given by

$$C \frac{dv}{dt} = i_L - g(v), \tag{1a}$$

$$L \frac{di_L}{dt} = -(Ri + R_s)i_L - v + F \sin(\Omega t), \tag{1b}$$

where $g(v)$ is the mathematical form of the piecewise-linear element given by

$$g(v) = G_b v + 0.5(G_b - G_a)[|v + B_p| - |v - B_p|]. \tag{2}$$

In terms of the rescaled parameters, the normalised state equations are given as

$$\dot{x} = y - g(x), \tag{3a}$$

$$\dot{y} = -\sigma y - \beta x + f \sin(\theta), \tag{3b}$$

$$\dot{\theta} = \omega, \tag{3c}$$

where $\sigma = (\beta + \nu\beta)$ and $\beta = (C/LG^2)$, $\nu = GR_s$, $a = G_a/G$, $b = G_b/G$, $f = (f\beta/B_p)$ and $\omega = (\omega C/G)$, $G = 1/R$. In the piecewise-linear form, $g(x)$ can be written as

$$g(x) = \begin{cases} bx + (a - b) & \text{if } x \geq 1, \\ ax & \text{if } |x| \leq 1, \\ bx - (a - b) & \text{if } x \leq -1. \end{cases} \tag{4}$$

The equations of system (3) are second order in each of the piecewise-linear regions. Hence, an explicit analytical solution can be obtained in each of these regions. The generalised analytical solutions for eq. (3) are summarised as follows.

In the central region D_0 , $g(x) = ax$ and the dynamical equation of the system is given as

$$\ddot{y} + A\dot{y} + By = af \sin(\omega t) + f\omega \cos(\omega t), \tag{5}$$

where $A = (\sigma + a)$ and $B = (\beta + a\sigma)$. The fixed points in the D_0 region are the origin $(0, 0)$. The stability of the fixed point in the D_0 region can be determined from the stability matrix

$$J_0 = \begin{pmatrix} -a & 1 \\ -\beta & -\sigma \end{pmatrix}. \tag{6}$$

When the roots of the above equation $m_{1,2} = (-A/2) \pm (\sqrt{A^2 - 4B})/2$ are real and distinct, then the state variables $y(t)$ and $x(t)$ are

$$y(t) = C_1 e^{m_1 t} + C_2 e^{m_2 t} + E_1 + E_2 \sin(\omega t) + E_3 \cos(\omega t), \tag{7a}$$

$$x(t) = \frac{1}{\beta} (-\sigma y - \dot{y} + f \sin(\omega t)). \tag{7b}$$

The constants of the particular integral E_1 , E_2 and E_3 are given as

$$E_1 = 0, \tag{8a}$$

$$E_2 = \frac{f\omega^2(A - a) + afB}{A^2\omega^2 + (B - \omega^2)^2}, \tag{8b}$$

$$E_3 = -\frac{f\omega(Aa + \omega^2 - B)}{A^2\omega^2 + (B - \omega^2)^2}. \tag{8c}$$

The constants of the complementary function C_1 and C_2 are given as

$$C_1 = \frac{e^{-m_1 t_0}}{m_1 - m_2} \{((\sigma - m_2)y_0 - \beta x_0 + m_2 E_1) + (m_2 E_3 - E_2 \omega) \cos \omega t_0 + (f + E_3 \omega + m_2 E_2) \sin \omega t_0\}, \quad (9a)$$

$$C_2 = \frac{e^{-m_2 t_0}}{m_2 - m_1} \{((\sigma - m_1)y_0 - \beta x_0 + m_1 E_1) + (m_1 E_3 - E_2 \omega) \cos \omega t_0 + (f + E_3 \omega + m_1 E_2) \sin \omega t_0\}. \quad (9b)$$

When the roots $m_{1,2}$ are a pair of complex conjugates, then $y(t)$ and $x(t)$ are given as

$$y(t) = e^{ut} (C_1 \cos vt + C_2 \sin vt) + E_1 + E_2 \sin(\omega t) + E_3 \cos(\omega t), \quad (10a)$$

$$x(t) = \frac{1}{\beta} (-\sigma y - \dot{y} + f \sin \omega t), \quad (10b)$$

where $u = -A/2$ and $v = (\sqrt{4B - A^2})/2$. The constants E_1, E_2 and E_3 are the same as given in eq. (8c) and the constants C_1 and C_2 are given as

$$C_1 = \frac{e^{-u t_0}}{v} \{((\sigma + u)y_0 + \beta x_0 - u E_1) \sin vt_0 + (y_0 - E_1)v \cos vt_0 - ((E_3 \omega + u E_2 + f) \sin vt_0 + v E_2 \cos vt_0) \sin \omega t_0 + ((E_2 \omega - u E_3) \sin vt_0 - v E_3 \cos vt_0) \cos \omega t_0\}, \quad (11a)$$

$$C_2 = \frac{e^{-u t_0}}{v} \{((\sigma + u)y_0 + \beta x_0 - u E_1) \cos vt_0 - (y_0 - E_1)v \sin vt_0 - ((E_3 \omega + u E_2 + f) \cos vt_0 - v E_2 \sin vt_0) \sin \omega t_0 + ((E_2 \omega - u E_3) \cos vt_0 + v E_3 \sin vt_0) \cos \omega t_0\}. \quad (11b)$$

In the $D_{\pm 1}$ region, $g(x) = bx \pm (a - b)$ and the dynamical equation can be written as

$$\ddot{y} + C\dot{y} + Dy = bf \sin(\omega t) + f\omega \cos(\omega t) \pm \Delta, \quad (12)$$

where $C = (\sigma + b)$, $D = (\beta + b\sigma)$ and $\Delta = \beta(a - b)$. The fixed points corresponding to the $D_{\pm 1}$ region are

$$\left(k_1 = \mp \frac{\sigma(a - b)}{(b\sigma + \beta)}, k_2 = \pm \frac{\beta(a - b)}{(b\sigma + \beta)} \right).$$

The stability of the fixed points corresponding to the $D_{\pm 1}$ regions can be determined from the stability matrix

$$J_0 = \begin{pmatrix} -b & 1 \\ -\beta & -\sigma \end{pmatrix}. \quad (13)$$

The state variables $y(t)$ and $x(t)$ in this region when the roots

$$m_{3,4} = \frac{-C}{2} \pm \frac{\sqrt{C^2 - 4D}}{2}$$

are real and distinct are given by

$$y(t) = C_3 e^{m_3 t} + C_4 e^{m_4 t} + E_4 + E_5 \sin(\omega t) + E_6 \cos(\omega t), \quad (14a)$$

$$x(t) = \frac{1}{\beta} (-\sigma y - \dot{y} + f \sin(\omega t)). \quad (14b)$$

The constants of the particular integral E_4, E_5 and E_6 are given as

$$E_4 = \pm \frac{\Delta}{D}, \quad (15a)$$

$$E_5 = \frac{f\omega^2(C - b) + bfD}{C^2\omega^2 + (D - \omega^2)^2}, \quad (15b)$$

$$E_6 = -\frac{f\omega(Cb + \omega^2 - D)}{C^2\omega^2 + (D - \omega^2)^2}. \quad (15c)$$

Here $+\Delta$ and $-\Delta$ correspond to D_{+1} and D_{-1} regions, respectively. The constants C_3 and C_4 are the same as given in eq. (9b) except that the constants a, A and B are replaced with b, C and D , respectively. When the roots $m_{3,4}$ are a pair of complex conjugates, the state variables are given as

$$y(t) = e^{ut} (C_3 \cos vt + C_4 \sin vt) + E_4 + E_5 \sin(\omega t) + E_6 \cos(\omega t), \quad (16a)$$

$$x(t) = \frac{1}{\beta} (-\sigma y - \dot{y} + f \sin \omega t), \quad (16b)$$

where $u = -C/2$ and $v = (\sqrt{4D - C^2})/2$. The constants C_3 and C_4 are the same as eq. (11b) except that the constants a, A and B are replaced with b, C and D , respectively. If we start with the initial condition in the D_0 region, the arbitrary constants C_1 and C_2 in eq. (7b) get fixed. Thus, $x(t)$ evolves as given in eq. (8c) up to either $t = T_1$ when $x(T_1) = 1$ and $\dot{x}(T_1) > 0$ or $t = T'_1$ when $x(T'_1) = -1$ and $\dot{x}(T'_1) < 0$. Knowing whether $T_1 < T'_1$ or $T_1 > T'_1$, we can determine the next region of interest ($D_{\pm 1}$) and the arbitrary constants of the solutions of that region can be fixed by matching the solutions. The procedure can be continued for each successive crossing. In this way, the explicit solutions can be obtained in each of the piecewise-linear regions D_0 and $D_{\pm 1}$. However, it is clear that the sensitive dependence on initial conditions is introduced in each of these crossings at appropriate parameter regimes during the inverse procedure of finding $T_1, T'_1, T_2, T'_2, \dots$, from the solutions.

The solutions presented above for each piecewise-linear regions can be used to obtain the trajectory of the

system in the corresponding region for a given initial condition (x_0, y_0) . The state variables (x, y) obtained every instant of time act as the initial condition for obtaining the state variables in the next instant. The state variables obtained in the individual regions can be plotted together to produce the complete phase-space trajectory. Now, we present the dynamics of series LCR circuit systems with two different types of nonlinear elements, using the analytical solutions obtained above.

2.1 Murali–Lakshmanan–Chua (MLC) circuit

The MLC circuit is a series LCR circuit with a Chua’s diode connected parallel to the capacitor. The circuit exhibits a wide range of chaotic behaviours in its dynamics. It has been studied for chaotic, strange non-chaotic and synchronisation behaviours for the past two decades [5,14,17]. The normalised values of the circuit parameters are given as $a = -1.02$, $b = -0.55$, $\beta = 1.0$, $\nu = 0.015$ and $\omega = 0.72$. The amplitude of the external force f is taken as the control parameter. The eigenvalues corresponding to the D_0 region are two real values while that of the $D_{\pm 1}$ regions are a pair of complex conjugates with negative real parts given by $\lambda_1 = 0.1904$, $\lambda_2 = -0.1854$ and $\lambda_{3,4} = -0.2325 \pm i0.623$, respectively. Hence, the origin is a saddle while the fixed points of the $D_{\pm 1}$ regions k_1 and k_2 are stable foci. When the amplitude of the external force $f = 0$, the trajectories starting from any initial condition near the origin deviate from it owing to its saddle nature as given by eqs (7b) and approach any one of the fixed point k_1 or k_2 as given by eqs (16b). As f is increased from zero, a stable limit cycle encompassing any one of the fixed points k_1 or k_2 depending upon the initial conditions is obtained. Further increase in f results in the period-doubling sequence of the limit cycle through the Hopf bifurcation leading to one-band and double-band chaotic attractors as shown in figure 4. The analytically obtained one-parameter bifurcation diagrams indicating the period-doubling and reverse period-doubling routes to chaos with f and ω as control parameters are shown in figures 2a and 2b, respectively. Figures 2c and 2d show the one-parameter bifurcation diagrams in the $f-x$ and $\omega-x$ planes obtained through numerical simulations. A comparison of the analytical and numerical results shown in figure 2 indicates that the dynamics of the system obtained analytically are identical to that obtained through numerical simulations. The analytical solutions can also be used to obtain the basins of attraction corresponding to one-band chaotic attractors. Figure 3a shows the basin of attraction corresponding to the one-band chaotic attractor in the (x_0-y_0) phase space. The green coloured regions indicate the set of initial conditions that settle down at the one-band

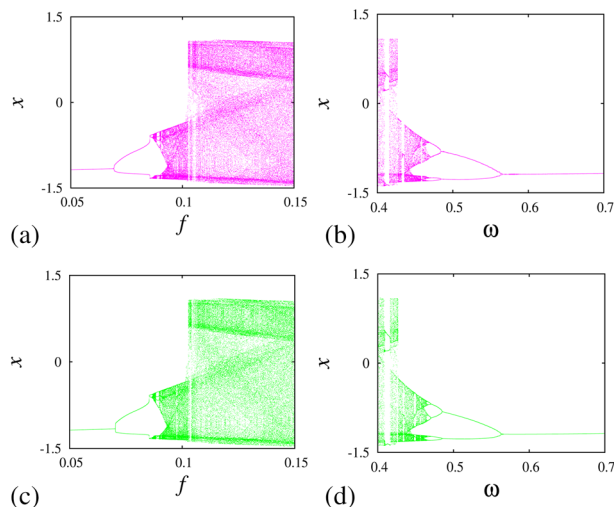


Figure 2. One-parameter bifurcation diagram of the MLC circuit obtained from the analytical solutions: (a) amplitude scanning in the $f-x$ plane with a fixed value of $\omega = 0.72$ and (b) frequency scanning in the $\omega-x$ plane with the amplitude fixed at $f = 0.053$. One-parameter bifurcation diagram of the MLC circuit obtained through numerical simulations: (c) amplitude scanning in the $f-x$ plane with a fixed value of $\omega = 0.72$ and (d) frequency scanning in the $\omega-x$ plane with the amplitude fixed at $f = 0.053$.

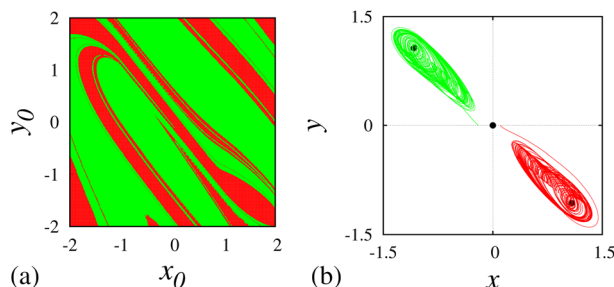


Figure 3. (a) Basins of attraction for the one-band chaotic attractor in the (x_0-y_0) phase-plane for the MLC circuit. The coloured regions are represented as follows: green – chaotic attractor corresponding to the left half-plane and red – chaotic attractor corresponding to the right half-plane. (b) One-band chaotic attractors originating from different initial conditions obtained from the basin of attraction near the fixed point $(0, 0)$.

chaotic attractor in the left half-plane of the phase space while the red coloured regions indicate the attractor corresponding to the right half-plane. Figure 3b shows the one-band chaotic attractors originating from the initial conditions corresponding to their coloured basins shown in figure 3a. The fixed points (black dots) in each of the piecewise-linear regions show that they form an attracting set in the phase space around which the one-band chaotic attractors settle down asymptotically. The analytical solutions can be further used to obtain the phase portraits and Poincare maps for the chaotic

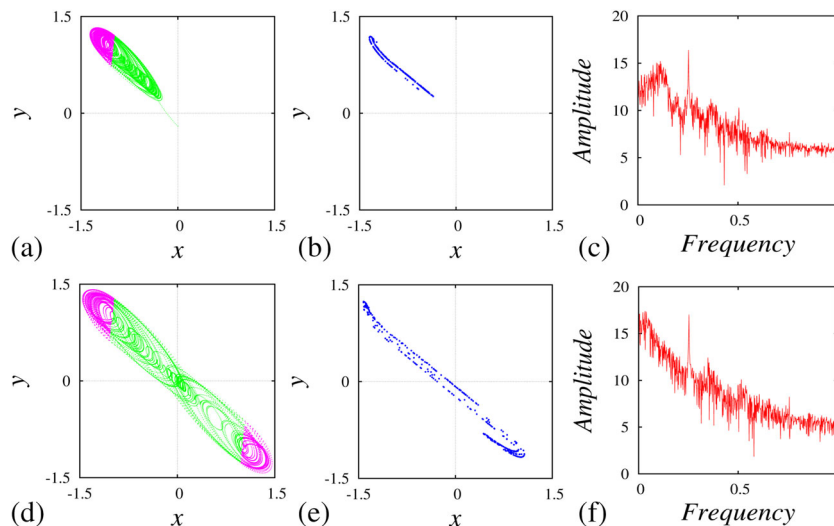


Figure 4. (a) One-band chaotic attractor in each of the piecewise linear regions D_0 (green) and D_{+1} (magenta) in the x - y phase-plane for the initial conditions $(x_0, y_0 = 0, -0.2)$, its corresponding (b) Poincare map, (c) power spectrum; (d) double-band chaotic attractor in the piecewise-linear regions D_0 (green) and $D_{\pm 1}$ (magenta) in x - y phase-plane, its corresponding (e) Poincare map and (f) power spectrum.

attractors as shown in figure 4. The state variables $x(t)$ and $y(t)$ obtained in each of the piecewise-linear regions are plotted to produce the chaotic attractors. The one-band chaotic attractor shown in figure 4a exists only in the D_{-1} and D_0 piecewise-linear regions. The Poincare maps and the power spectra indicating a broader range of frequency distribution corresponding to the one-band chaotic attractor are shown in figures 4b and 4b, respectively. The phase portrait, Poincare map and power spectrum corresponding to the double-band chaotic attractor are shown in figures 4d–4f.

2.2 Forced series LCR circuit with a simplified nonlinear element

This circuit introduced by Arulgnanam *et al* [6] produces chaotic attractors with a least number of circuit elements. Further, the fractal dimension of the chaotic attractors observed in this system is found to have a larger value compared to the other second-order chaotic systems. Figure 5 shows the experimentally observed chaotic attractor in the $(v - i_L)$ phase-plane for the circuit parameters $C = 10.32$ nF, $L = 42.6$ mH, $R = 2050$ Ω , $G_a = -0.56$ mS, $G_b = +2.5$ mS, $B_p = \pm 1.0$ V and $F = 4.59$ V. The circuit also exhibits a wide range of chaotic behaviours similar to the MLC circuit. The eigenvalues corresponding to the D_0 region are two real values with one negative value and one positive value while that of the $D_{\pm 1}$ regions are two negative real values given by $\lambda_1 = 0.47126$, $\lambda_2 = -0.30976$ and $\lambda_3 = -1.24075$, $\lambda_4 = -4.87075$, respectively. Hence, the origin is a saddle while the fixed points of the $D_{\pm 1}$ regions k_1 and k_2 are stable nodes. When

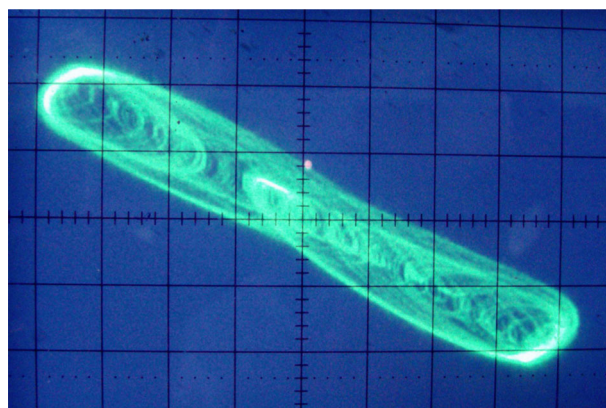


Figure 5. Experimentally observed double-band chaotic attractor in the forced series LCR circuit with a simplified nonlinear element in the v - i_L phase-plane.

the amplitude of the external force $f = 0$, trajectories arising from the initial conditions near the origin deviate from the origin exponentially as given by eq (7b) and approach any one of the fixed points k_1 or k_2 exponentially, as given by eq. (12). On increasing f , a stable limit cycle is obtained which results in period-doubling sequences through the Hopf bifurcation for further increase in f . The normalised circuit parameter values are $a = -1.148$, $b = 5.125$, $\beta = 0.9865$, $\nu = 0$ and $\omega = 0.7084$. The analytically obtained one-parameter bifurcation diagrams in the f - x and ω - x planes indicating the period-doubling and reverse period-doubling sequences observed in the circuit dynamics are shown in figures 6a and 6b, respectively. The analytically obtained basins of attraction for the one-band chaotic attractors shown in figure 7a indicate the set of initial conditions

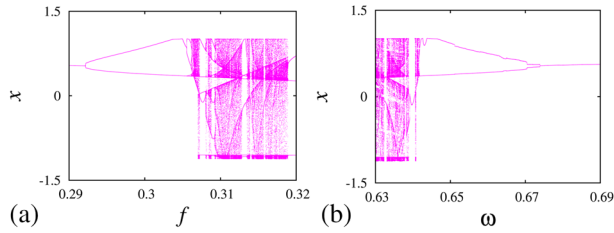


Figure 6. One-parameter bifurcation diagram of the forced series LCR circuit with a simplified nonlinear element: **(a)** amplitude scanning in the f - x plane with a fixed value of $\omega = 0.7084$ indicating the period-doubling route to chaos and **(b)** frequency scanning in the ω - x plane with the amplitude fixed at $f = 0.28$.

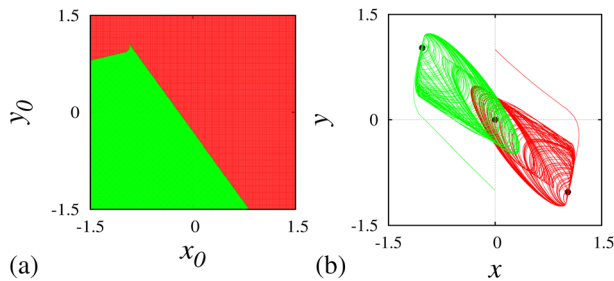


Figure 7. **(a)** Basins of attraction for the one-band chaotic attractor in the $(x_0$ - $y_0)$ phase-plane for the series LCR circuit with a simplified nonlinear element. The coloured regions are represented as follows: green – chaotic attractor corresponding to the left half-plane and red – chaotic attractor corresponding to the right half-plane. **(b)** One-band chaotic attractors originating from different initial conditions obtained from the basin of attraction.

that settle down into a one-band chaotic attractor at the right half-plane (red) and the left half-plane (green). The one-band chaotic attractors arising from two different coloured basins shown in figure 7a along with the fixed points (black dots) of the three piecewise-linear regions are shown in figure 7b. The analytically observed one-band chaotic attractor in the piecewise-linear regions and its corresponding Poincare map and power spectrum obtained at the amplitude of the external force $f = 0.3065$ are shown in figures 8a–8c. Figures 8d–8f show the double-band chaotic attractor and its corresponding Poincare map and power spectrum obtained when amplitude $f = 0.31$.

3. Analytical dynamics of the parallel LCR circuit systems

The state equations of a forced parallel LCR circuit system with a three-segmented piecewise-linear element connected parallel to the capacitor are given as

$$C \frac{dv}{dt} = \frac{1}{R}(F \sin(\Omega t) - v) - i_L - g(v), \quad (17a)$$

$$L \frac{di_L}{dt} = v. \quad (17b)$$

The piecewise-linear function $g(v)$ is as given in eq. (2). After proper rescaling, the normalised state equations of the system can be written as

$$\dot{x} = f \sin(\theta) - x - y - g(x), \quad (18a)$$

$$\dot{y} = \beta x, \quad (18b)$$

$$\dot{\theta} = \omega, \quad (18c)$$

where $x = v/B_p$, $y = (i_L/GB_p)$, $\beta = (C/LG^2)$, $a = G_a/G$, $b = G_b/G$, $f = (F\beta/B_p)$, $\omega = (\Omega C/G)$ and $G = 1/R$. The mathematical form of the function $g(x)$ is given in eq. (4). The explicit analytical solutions obtained for the normalised state equations given in eq. (18c) are summarised as follows.

In the central region D_0 , $g(x) = ax$ and the dynamical equations of the system can be written as

$$\ddot{y} + A\dot{y} + By = f\beta \sin(\omega t), \quad (19)$$

where $A = 1 + a$ and $B = \beta$. The stability of the fixed point $(0, 0)$ in the D_0 region can be determined from the stability matrix

$$J_0 = \begin{pmatrix} -(1+a) & -1 \\ -\beta & 0 \end{pmatrix}. \quad (20)$$

The state variables of the system when the roots

$$m_{1,2} = \frac{-(A) \pm \sqrt{A^2 - 4B}}{2}$$

are real and distinct are given by

$$y(t) = C_1 e^{m_1 t} + C_2 e^{m_2 t} + E_1 + E_2 \sin(\omega t) + E_3 \cos(\omega t), \quad (21a)$$

$$x(t) = \frac{1}{\beta}(\dot{y}). \quad (21b)$$

The constants E_1 , E_2 and E_3 are given as

$$E_1 = 0, \quad (22a)$$

$$E_2 = \frac{f\beta(B - \omega^2)}{A^2\omega^2 + (B - \omega^2)^2}, \quad (22b)$$

$$E_3 = -\frac{fA\beta\omega}{A^2\omega^2 + (B - \omega^2)^2}. \quad (22c)$$

The constants C_1 and C_2 are given as

$$C_1 = \frac{e^{-m_1 t_0}}{m_1 - m_2} \{ (\beta x_0 - m_2 y_0 + m_2 E_1) + (m_2 E_3 - \omega E_2) \cos \omega t_0 + (\omega E_3 + m_2 E_2) \sin \omega t_0 \}, \quad (23a)$$

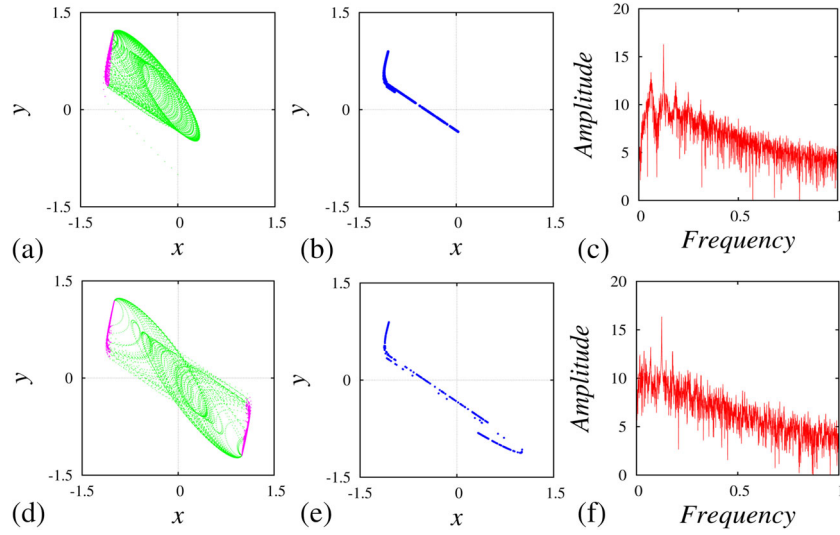


Figure 8. (a) One-band chaotic attractor in each of the piecewise linear regions D_0 (green) and D_{+1} (magenta) in the x - y phase-plane for the initial conditions $(x_0, y_0 = 0, -1)$ and its corresponding (b) Poincaré map and (c) power spectrum; (d) double-band chaotic attractor in the piecewise-linear regions D_0 (green) and $D_{\pm 1}$ (magenta) in the x - y phase-plane and its corresponding (e) Poincaré map and (f) power spectrum.

$$C_2 = \frac{e^{-m_2 t_0}}{m_2 - m_1} \{ (\beta x_0 - m_1 y_0 + m_1 E_1) + (m_1 E_3 - \omega E_2) \cos \omega t_0 + (\omega E_3 + m_1 E_2) \sin \omega t_0 \}. \quad (23b)$$

When the roots are a pair of complex conjugates, then the state variables are

$$y(t) = e^{ut} (C_1 \cos vt + C_2 \sin vt) + E_1 + E_2 \sin \omega t + E_3 \cos \omega t, \quad (24a)$$

$$x(t) = \frac{1}{\beta} (\dot{y}), \quad (24b)$$

where $u = -A/2$ and $v = (\sqrt{4B - A^2})/2$. The constants C_1 and C_2 are given as

$$C_1 = -\frac{e^{-u t_0}}{v} \{ ((\beta x_0 - u y_0 + u E_1) \sin vt_0 - v y_0 \cos vt_0 - ((E_2 \omega - u E_3) \sin vt_0 - v E_3 \cos vt_0) \cos \omega t_0 + ((E_3 \omega + u E_2) \sin vt_0 + v E_2 \cos vt_0) \sin \omega t_0 \}, \quad (25a)$$

$$C_2 = -\frac{e^{-u t_0}}{v} \{ ((\beta x_0 - u y_0 + u E_1) \cos vt_0 + v y_0 \sin vt_0 - ((E_2 \omega - u E_3) \cos vt_0 + v E_3 \sin vt_0) \cos \omega t_0 + ((E_3 \omega + u E_2) \cos vt_0 - v E_2 \sin vt_0) \sin \omega t_0 \}. \quad (25b)$$

In the $D_{\pm 1}$ regions, $g(x) = bx \pm (a - b)$ and the dynamical equation of the system can be written as

$$\ddot{y} + C\dot{y} + Dy = f\beta \sin(\omega t) \mp \Delta, \quad (26)$$

where $C = (1 + b)$, $D = \beta$ and $-\Delta$ and $+\Delta$ correspond to the D_{+1} and D_{-1} regions, respectively. The fixed points in the $D_{\pm 1}$ regions are $k_{1,2} = (0, \pm b - a)$. The stability of the fixed points in this region can be determined using the stability matrix

$$J_{\pm 1} = \begin{pmatrix} -(1 + b) & -1 \\ -\beta & 0 \end{pmatrix}. \quad (27)$$

The state variables in these regions when the roots

$$m_{3,4} = \frac{-C}{2} \pm \frac{\sqrt{C^2 - 4D}}{2}$$

are real and distinct are given as

$$y(t) = C_3 e^{m_3 t} + C_4 e^{m_4 t} + E_4 + E_5 \sin \omega t + E_6 \cos \omega t \pm \Delta, \quad (28a)$$

$$x(t) = \frac{1}{\beta} (\dot{y}). \quad (28b)$$

The constants E_4 , E_5 and E_6 are given as

$$E_4 = \mp \Delta, \quad (29a)$$

$$E_5 = \frac{f\beta(D - \omega^2)}{C^2 \omega^2 + (D - \omega^2)^2}, \quad (29b)$$

$$E_6 = -\frac{Df\beta\omega}{C^2 \omega^2 + (D - \omega^2)^2}. \quad (29c)$$

The constants C_3 and C_4 are the same as eq. (23b) except that the constants a , A and B are replaced with b , C and D , respectively. When the roots $m_{3,4}$ are a pair of complex conjugates, the state variables are given as

$$y(t) = e^{ut} (C_3 \cos vt + C_4 \sin vt) + E_4 + E_5 \sin(\omega t) + E_6 \cos(\omega t) \pm \Delta, \tag{30a}$$

$$x(t) = \frac{1}{\beta} (\dot{y}), \tag{30b}$$

where $u = -C/2$ and $v = (\sqrt{4D - C^2})/2$. The constants C_3 and C_4 are the same as eq. (25b) except that the constants a, A and B are replaced with b, C and D , respectively. The solutions obtained can be used to generate the trajectories of the state variables as explained in §2. Now, we discuss the analytical dynamics of the parallel LCR circuit systems with the Chua’s diode and the simplified nonlinear element as the nonlinear elements.

3.1 Variant of MLC (MLCV) circuit

The MLCV circuit introduced by Thamilmaran *et al* [7] presents a rich variety of bifurcations and chaos

in its dynamics such as the quasiperiodic, reverse period-doubling routes to chaos, antimonotonicity and remerging Feignbaum trees to name a few [16]. Using the analytical solutions presented above, we discuss some of the bifurcation and chaotic phenomena observed in the circuit dynamics. The eigenvalues corresponding to the D_0 and $D_{\pm 1}$ regions are given as $\lambda_{1,2} = 0.635 \pm i0.2144$ and $\lambda_{3,4} = -0.19762 \pm 0.623$, respectively. Hence, the origin is an unstable focus while the fixed points corresponding to the $D_{\pm 1}$ regions k_1 and k_2 are stable foci fixed points. When the amplitude of the external force $f = 0$, the asymptotic divergence of the trajectories starting from initial conditions near the origin as observed by eqs (24b) is balanced by the asymptotic convergence solutions in the $D_{\pm 1}$ regions given by eqs (30b), as the trajectories cross the breaking point regions $B_p = \pm 1$. Hence, a stable limit cycle occupying a fixed region in the phase space is observed in the circuit dynamics when $f = 0$. On the application of the external force, an invariant torus is obtained through the Hopf bifurcation of the limit cycle because of its interaction with the external force. On increasing f , a chaotic attractor emerges through the destruction of this invariant torus. The analytically obtained one-parameter bifurcation diagram in the $f-x$ plane shown in figure 9a reveals the antimonotonicity behaviour observed in the dynamics of the circuit. The period-doubling route to chaos leads to a reverse period-doubling sequence with the increase in the amplitude of the external force f as shown in figure 9a. Figure 9b shows the one-parameter bifurcation diagram obtained in the $\omega-x$ plane. Another interesting phenomenon named the remerging Feignbaum trees observed numerically in the circuit dynamics

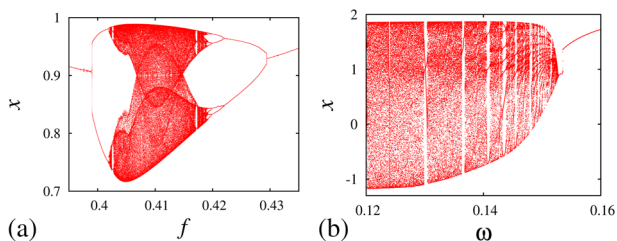


Figure 9. One-parameter bifurcation diagram of the MLCV circuit: (a) amplitude scanning in the $f-x$ plane with a fixed value of $\omega = 0.105$. The period-doubling route to chaos followed by a reverse period-doubling route indicates antimonotonicity behaviour and (b) frequency scanning in the $\omega-x$ plane with the amplitude fixed at $f = 0.225$.

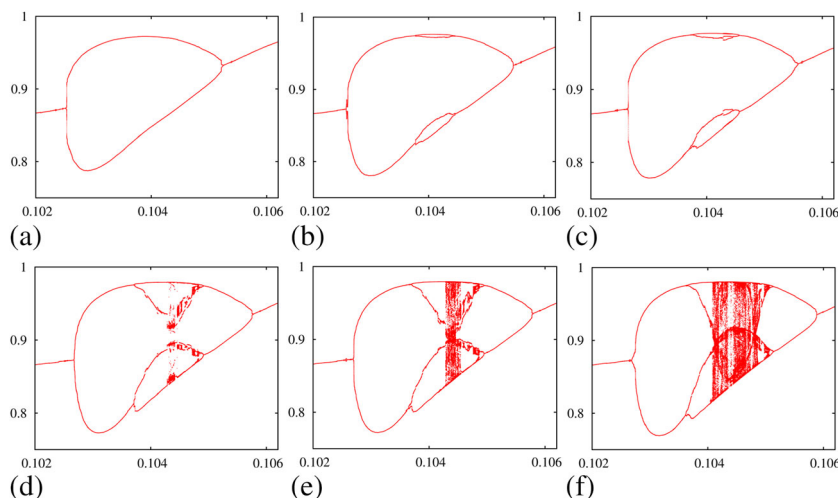


Figure 10. One-parameter bifurcation diagram in the $\omega-x$ plane indicating the remerging Feignbaum trees phenomena in the MLCV circuit. The amplitude of the external force is taken as the control parameter: (a) the primary bubble at $f = 0.429$, (b) period-4 bubble at $f = 0.4275$, (c) period-8 bubble at $f = 0.4271$. Further decrease in the amplitude results in infinite period bubbles and undergo Feignbaum remerging tree at (d) $f = 0.42585$, (e) $f = 0.4257$ and (f) $f = 0.425$.

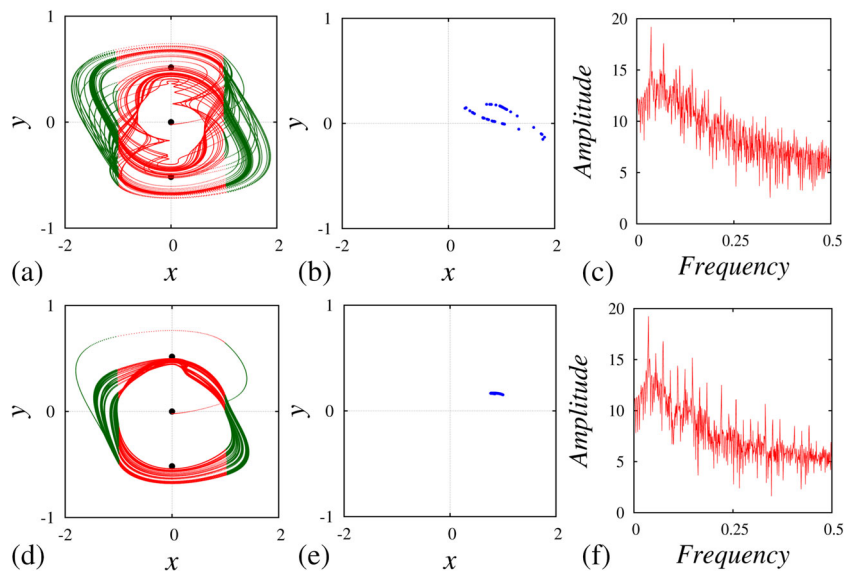


Figure 11. (a) Chaotic attractor observed at $f = 0.375$ in each of the piecewise linear regions D_0 (red) and $D_{\pm 1}$ (green) in the x - y phase-plane for the initial conditions $(x_0, y_0) = (0, 0)$ and its corresponding (b) Poincaré map and (c) power spectrum; (d) chaotic attractor observed at $f = 0.411$ in the x - y phase-plane and its corresponding (e) Poincaré map and (f) power spectrum.

[16] is explained using the analytically obtained one-parameter bifurcation diagrams shown in figure 10. Further, a plot of the analytical solutions of each piecewise-linear regions results in chaotic attractors, as shown in figures 11a and 11d, for the amplitudes $f = 0.375$ and $f = 0.411$, respectively. The chaotic attractors settle down in the region of space around the unstable and stable fixed points (black dots) of the D_0 and $D_{\pm 1}$ regions, respectively. The Poincaré map and the power spectrum of the chaotic attractors shown in figures 11a and 11d are presented in figures 11b, 11c and 11e, 11f, respectively.

3.2 Forced parallel LCR circuit with a simplified nonlinear element

The forced parallel LCR circuit with a simplified nonlinear element introduced by Arulgnanam *et al* [8] exhibits a torus breakdown and reverse period-doubling routes to chaos. In this circuit, the fixed points corresponding to the D_0 region are an unstable focus while those corresponding to the $D_{\pm 1}$ regions are stable nodes. The eigenvalues corresponding to the D_0 and $D_{\pm 1}$ regions are given as $\lambda_{1,2} = 0.074 \pm i0.50371$ and $\lambda_3 = -0.04261, \lambda_4 = -6.0824$, respectively. Hence, the dynamics of this circuit resembles that of the MLCV circuit. When $f = 0$, a stable limit cycle encompassing the origin is obtained. Further increase in f leads to the torus breakdown route to chaos. The circuit exhibits two prominent chaotic attractors at the amplitudes of the external force $F = 4.75$ and

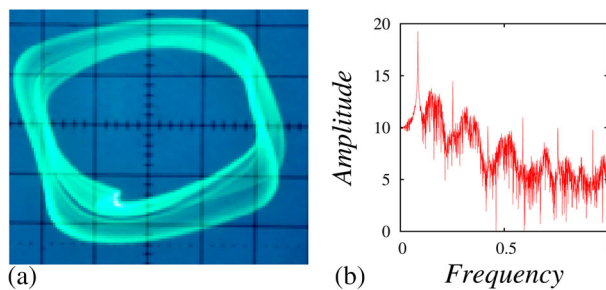


Figure 12. (a) Experimentally observed chaotic attractor in the forced parallel LCR circuit with a simplified nonlinear element in the v - i_L phase-plane at $F = 4.779$ V and its corresponding (b) analytically observed power spectrum.

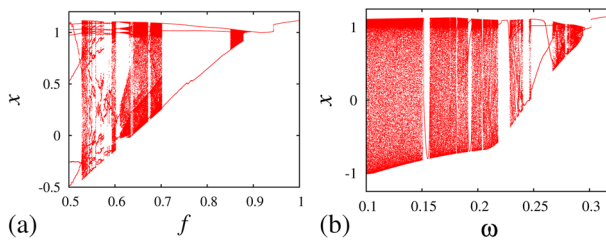


Figure 13. One-parameter bifurcation diagram for the forced parallel LCR circuit with a simplified nonlinear element: (a) amplitude scanning in the f - x plane with a fixed value of $\omega = 0.2402$ showing the entire dynamics of the circuit and (b) frequency scanning in the ω - x plane with the amplitude fixed at $f = 0.6$.

$F = 4.779$ with other circuit parameters fixed at $C = 13.13$ nF, $L = 163.6$ mH, $R = 2.05$ k Ω , $G_a = -0.56$ mS, $G_b = +2.5$ mS and $B_p = \pm 3.8$ V,

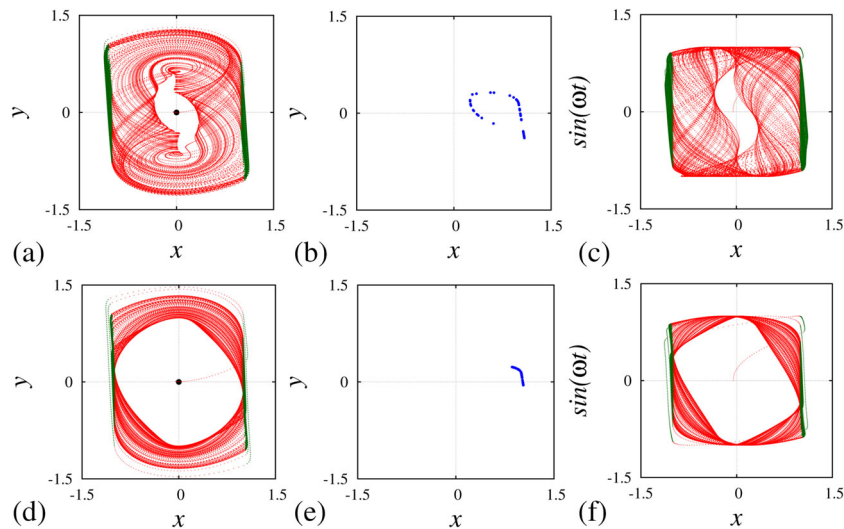


Figure 14. (a) Chaotic attractor observed at $f = 0.695$ in each of the piecewise linear regions D_0 (red) and $D_{\pm 1}$ (green) in the x - y phase-plane for the initial conditions $(x_0, y_0) = (0, 0)$ and its corresponding (b) Poincaré map and (c) chaotic attractor in the x - $\sin(\omega t)$ plane; (d) chaotic attractor observed at $f = 0.855$ in the x - y phase-plane and its corresponding (e) Poincaré map and (f) chaotic attractor in the x - $\sin(\omega t)$ plane.

respectively. The rescaled parameters of the circuit are: $\beta = 0.2592$, $a = -1.148$, $b = 5.125$ and $\nu = 1.421$ kHz. The experimentally observed chaotic attractor and its corresponding analytically observed power spectra are shown in figure 12. The entire dynamics of the circuit observed analytically through one-parameter bifurcation diagrams in the $(f-x)$ and $(\omega-x)$ planes are shown in figures 13a and 13b, respectively. From figure 13, we can observe that the circuit exhibits chaotic behaviour over a wide range of amplitude and frequency of the external force. Figures 14a and 14d show the analytically obtained chaotic attractors plotted in each of the piecewise-linear region D_0 (red) and $D_{\pm 1}$ (green) for $f = 0.695$ and $f = 0.855$, respectively. The Poincaré map of the chaotic attractors shown in figures 14a and 14d are shown in figures 14b, 14e and the phase portraits of the chaotic attractors in x - $\sin(\omega t)$ phase planes are shown in figures 14c, 14f, respectively.

4. Conclusions

In this paper, we have reported the effective application of an analytical solution for identifying several interesting phenomena in simple chaotic systems. The anti-monotonicity, period-doubling, reverse period-doubling and Feigenbaum remerging identified earlier through numerical studies have been proved analytically. Phase portraits revealing the existence of trajectories in individual piecewise-linear regions have been presented. The efficiency of this solution can be applied for studying the dynamics of second-order chaotic circuit systems with five or more segmented piecewise-linear elements,

analytically. Further, the reliability of the analytical solutions has been well established through its identical behaviour with the numerical results. Explicit analytical solutions of this kind pave way for a better understanding of the chaotic phenomena observed in simple circuit systems.

Acknowledgements

One of the authors A Arulgnanam gratefully acknowledges Dr K Thamilmaran, the Centre for Nonlinear Dynamics, Bharathidasan University, Tiruchirapalli, for his help and permission to carry out the experimental work during his doctoral programme.

References

- [1] M J Ogorzalek, *IEEE Trans. Circuits Syst. I* **40**, 693 (1993)
- [2] M Lakshmanan and K Murali, *Curr. Sci.* **67**, 989 (1994)
- [3] M Lakshmanan and S Rajasekar, *Nonlinear dynamics: Integrability, chaos and patterns* (Springer, Berlin, 2003)
- [4] T Matsumoto, *IEEE Trans. Circuits Syst.* **31**, 1055 (1984)
- [5] K Murali, M Lakshmanan and L O Chua, *IEEE Trans. Circuits Syst.* **41**, 462 (1994)
- [6] A Arulgnanam, K Thamilmaran and M Daniel, *Chaos Solitons Fractals* **42**, 2246 (2009)
- [7] K Thamilmaran, M Lakshmanan and K Murali, *Int. J. Bifurc. Chaos* **10**, 1175 (2000)
- [8] A Arulgnanam, K Thamilmaran and M Daniel, *Chin. J. Phys.* **53**, 060702 (2015)

- [9] B C Lai and J J He, *Pramana – J. Phys.* **90**: 33 (2018)
- [10] P M Ezhilarasu, M Inbavalli, K Murali and K Thamilmaran, *Pramana – J. Phys.* **91**: 4 (2018)
- [11] M P Kennedy, *Frequenz* **46**, 66 (1992)
- [12] J G Lacy, *Int. J. Bifurc. Chaos* **6**, 2097 (1996)
- [13] M Lakshmanan and K Murali, *Phil. Trans: Phys. Sci. Eng.* **353**, 1701 (1995)
- [14] G Sivaganesh, *Chin. J. Phys.* **52**, 1760 (2014)
- [15] G Sivaganesh and A Arulgnanam, *J. Korean Phys. Soc.* **69**, 1631 (2016)
- [16] K Thamilmaran and M Lakshmanan, *Int. J. Bifurc. Chaos* **12**, 783 (2001)
- [17] G Sivaganesh, *Chin. Phys. Lett.* **32**, 010503 (2015)
- [18] P R Venkatesh, A Venkatesan and M Lakshmanan, *Pramana – J. Phys.* **86**, 1195 (2016)
- [19] G Sivaganesh and A Arulgnanam, *Chin. Phys. B* **26(5)**, 050502 (2017)
- [20] G Sivaganesh, A Arulgnanam and A N Seethalakshmi, *Chaos Solitons Fractals* **113**, 294 (2018)